CMLS, Cell. Mol. Life Sci. 61 (2004) 2100–2112
1420-682X/04/162100-13
DOI 10.1007/s00018-004-4222-9

CMLS Cellular and Molecular Life Sciences

Research Article

Infection of cultured intestinal epithelial cells with severe acute respiratory syndrome coronavirus

J. Cinatl Jr.[a,*], G. Hoever[a], B. Morgenstern[a], W. Preiser[a], J.-U. Vogel, W.-K. Hofmann[b], G. Bauer[a], M. Michaelis[a], H. F. Rabenau[a] and H. W. Doerr[a]

[a] Institute for Medical Virology, Johann Wolfgang Goethe University Hospital, Paul-Ehrlich Str. 40, 60596 Frankfurt am Main (Germany), Fax +49 69 6301 4302, e-mail: Cinatl@em.uni-frankfurt.de
[b] Department of Haematology and Oncology, Johann Wolfgang Goethe University Hospital, Frankfurt am Main (Germany)

Received 23 May 2004; received after revision 23 June 2004; accepted 25 June 2004

Abstract. To identify a model for the study of intestinal pathogenesis of severe acute respiratory syndrome (SARS) we tested the sensitivity of six human intestinal epithelial cell lines to infection with SARS coronavirus (SARS-CoV). In permissive cell lines, effects of SARS-CoV on cellular gene expression were analysed using high-density oligonucleotide arrays. Caco-2 and CL-14 cell lines were found to be highly permissive to SARS-CoV, due to the presence of angiotensin-converting enzyme 2 as a functional receptor. In both cell lines, SARS-CoV infection deregulated expression of cellular genes which may be important for the intestinal pathogenesis of SARS.

Key words. SARS, SARS-CoV; coronavirus; intestine; Caco-2; CL-14, microarray.

Severe acute respiratory syndrome (SARS) is caused by infection with the SARS coronavirus (SARS-CoV) [1]. Approximately 25% of patients with SARS are likely to progress to severe respiratory failure with characteristics of acute respiratory distress syndrome [2].

Although the pathogenesis of SARS is still unclear, it is believed that after binding to its functional receptor, i.e. angiotensin-converting enzyme 2 (ACE2), SARS-CoV replicates in permissive cells resulting in their lysis [3]. Therefore, damage of infected tissue may result directly from virus replication (cytolytic activity). On the other hand, the progression of SARS to respiratory failure in the later phase of the disease (weeks 2 and 3) which occurs in a notable proportion of patients despite lowering of virus load suggests an immunopathological mechanism [4].

Gastrointestinal symptoms are frequently observed in patients with SARS. In the Hong Kong and Toronto outbreaks, a considerable proportion of patients had watery diarrhoea, sometimes preceding the onset of respiratory symptoms [5, 6]. Peiris et al. [4] reported that up to 70% of their patients in the community outbreak in Hong Kong developed watery diarrhea. Patients with diarrhea had higher rates of intensive care unit admission and intubation; however, there was no association with oxygen requirement and overall mortality [5, 7]. Despite a relatively normal endoscopic and microscopic appearance of the gut in SARS patients with gastrointestinal involvement, SARS-CoV was found in the large and small bowel by both electron microscopy and viral culture [5].

We previously demonstrated that the intestinal Caco-2 cell line is highly permissive to SARS-CoV infection [8]. In the present study, we compared the sensitivity of Caco-2 cells to SARS-CoV infection with that of five other human intestinal cell lines. Only the CL-14 cell line was

* Corresponding author.

highly sensitive to SARS-CoV. Both Caco-2 and CL-14 were used to define the effects of SARS-CoV infection on the cellular gene expression profile.

Materials and methods

Cell cultures

Human cell lines derived from colon carcinoma including Caco-2, CL-14, HT-29, SW-480, DLD-1 and HCT-15 were obtained from the Deutsche Sammlung von Mikroorganismen und Zellkulturen (DSMZ; Braunschweig, Germany). The cells were grown at 37 °C in Iscove's modified Dulbecco's medium (IMDM) supplemented with 10% fetal bovine serum (FBS) and containing 100 IU/ml of penicillin and 100 µg/ml of streptomycin. All culture reagents were purchased from Biochrom (Berlin, Germany).

Virus preparation

SARS-CoV strain FFM-1 was isolated from respiratory specimens of a SARS patient admitted to the Infectious Diseases Department of Frankfurt am Main University Hospital, Germany, on Vero (African green monkey kidney; ATCC CCL81) cells [9]. SARS-CoV strain 6109 (courtesy of Prof. W. Lim, Government Virus Unit, Hong Kong) was obtained from a Hong Kong patient early in the outbreak there and is thus one transmission generation earlier than the FFM-1 strain. SARS-CoV stocks used in the experiments had undergone five passages on Vero cells and were stored at –80 °C. Virus titers were determined as $TCID_{50}$/ml in confluent cells in 96-well microtitre plates [9].

Immune staining of viral antigens

Cells infected with SARS-CoV at multiplicity of infection (MOI) 1 and MOI 10 were collected at different times post infection (p.i.) by trypsinization of adherent cells. Non-adherent cells (the numbers of which increased with time after infection) were collected by centrifugation of culture supernatants. Both adherent and non-adherent cells were fixed on glass slides with 60/40 methanol/acetone for 15 min. Immune peroxidase staining was performed using human immune serum obtained from a SARS patient as described previously [9].

SARS-CoV receptor blocking experiments

To investigate whether ACE2 is a functional receptor for SARS-CoV in intestinal epithelial cell cultures, the cells were pre-treated for 60 min at 37 °C with goat antibody directed against the human ACE2 ectodomain (R&D Systems; Wiesbaden-Nordenstadt, Germany). After treatment, the cells were washed three times with phosphate-buffered saline (PBS) and infected with one of the SARS-CoV strains at MOI 1. Twenty-four hours p.i. the cells were fixed and stained for viral antigens as described above. Goat anti-ACE1 antibody (R&D Systems) was used as control. Both antibodies were added at a concentration of 50 µg/ml.

Flow cytometry

To investigate expression of cell surface ACE2, intestinal cell lines were washed twice with PBS and incubated for 30 min with goat anti-ACE2 antibody (R&D Systems). After washing with PBS, the cells were incubated with FITC-conjugated anti-goat IgG (Becton Dickinson, Heidelberg, Germany) for 30 min. As controls, cells were stained with irrelevant primary antibody (goat anti-mouse IgG; Sigma Biochemicals, Seelze, Germany) or without a primary antibody to determine unspecific and background fluorescence, respectively. Instrument settings of the flow cytometer (FACScan; Becton Dickinson) were adjusted to obtain background mean fluorescence in the histogram mode between 1 and 10 on the logarithmic scale.

Electron microscopy

Caco-2 cells were infected 2–3 days after reaching confluence with SARS-CoV at MOI 1. One day p.i., the cells were processed for ultrastructural analysis as described previously [10]. Briefly, cells were pelleted and fixed with 2.5% glutaraldehyde, post-fixed in 1% osmium tetroxide, dehydrated in ethanol and embedded in Durupan-Epon. Thin sections were contrasted with uranyl acetate and lead citrate and viewed with a Jeol JEM, 2000 CX electron microscope (Arishima, Japan).

Cell viability assay

To assess effects of SARS-CoV infection on Caco-2 cell viability, confluent cell layers in 96-well plates were infected at MOI 1 and MOI 10. The viability was measured at different times p.i. using the MTT assay performed as described previously [10].

Gene expression analysis by oligonucleotide microarrays and RT-PCR

Gene array analysis was done according to the principles of Miame [11] We used the Affymetrix HG-U133A chip (Affymetrix, Santa Clara, Calif.). This oligonucleotide microarray targets 22,000 genes. Sample preparation was done by the RNeasy Mini Kit (Qiagen, Hilden, Germany) standard protocol. Generation of biotin-labelled cRNA, hybridization and staining were done according to standard protocols available from Affymetrix. Data analysis was performed using Microarray Analysis Suite (Affymetrix) and GeneSpring software version 4.0 (Silicon Genetics, San Carlos, Calif.) as published previously [12]. In brief, the lowest raw data value was arbitrarily defined as '11' in order not to eliminate genes which are expressed only in one sample. To eliminate false

'fold-change' calls, genes that were classified as 'up-regulated' had to be flagged as 'present' in the infected samples, while genes that were classified as 'down-regulated' had to be flagged as 'present' in the mock-infected samples. Within those parameters, genes were selected if they were either up- or down-regulated at least threefold in duplicate. Following microarray analysis, genes related to apoptosis, cytokines, chemokines or interferons were confirmed by RT-PCR, according to standard protocols [10]. PCR primer and amplification conditions were determined by the software Primer3 (Whitehead Institute for Biomedical Research, Cambridge, Mass.) [13].

Results

Virus growth

Previously, we demonstrated that Caco-2 cells are highly permissive to infection with SARS-CoV strain FFM-1 [8]. In the present study we extended our observations by comparing the sensitivity of Caco-2 cells to SARS-CoV with that of five other intestinal cell lines including CL-14, HT-29, SW-480, DLD-1 and HCT-15. In addition to strain FFM-1, the sensitivity of intestinal cell lines to infection with SARS-CoV strain 6109 was tested. Caco-2 and CL-14 cells were the only cell lines permissive to infection with both SARS-CoV strains. In Caco-2 cells infected with the FFM-1 strain at MOI 1, infectious virus titers increased from none at 1 h p.i. to a maximum of 5.4×10^7 $TCID_{50}$/ml at 48 h p.i. (fig. 1A). Infection of Caco-2 cells at MOI 10 resulted in 10-fold (1.5×10^6 vs 1.1×10^5 $TCID_{50}$/ml) and 4-fold (8.3×10^7 vs 2.1×10^7 $TCID_{50}$/ ml) higher infectious titers 12 and 24 h p.i. relative to cultures infected at MOI 1. The maximum virus titers in cultures infected at MOI 10 were similar to those of cultures infected at MOI 1 (8.3×10^7 vs 5.4×10^7 $TCID_{50}$/ml); however, the maximum was already achieved at 24 h p.i. (fig. 1A).

In CL-14 cells infected at MOI 1 with the FFM-1 strain, a maximum virus titer of 3.7×10^7 $TCID_{50}$/ml was measured 72 h p.i., i.e. 1 day later than in Caco-2 cells (fig. 1B). In CL-14 cultures infected at MOI 10, a maximum virus titer of 4.5×10^7 $TCID_{50}$/ml had already developed 48 h p.i. (fig. 1B).

In both Caco-2 and CL-14 cells infected at MOI 1, a cytopathic effect (CPE) did not appear before 48 h p.i. The CPE at 72 h p.i. was very marked, with numerous rounded and enlarged cells, some of which became detached (fig. 2A). Although most of the cells stained positive for viral antigens 72 h p.i., the exact numbers of infected cells could not be determined due to the extensive cellular lysis. Some cells which were not destroyed continued to adhere to the culture vessel surface and did not stain with immune serum (fig. 2A). For both cell lines, the CPE developed 1 day earlier in cultures infected at MOI 10 than in those infected at MOI 1.

Infection of Caco-2 and CL-14 cells with the SARS-CoV 6109 strain resulted in a similar viral titer and similar CPE when compared with cells infected with the FFM-1 strain (data not shown).

Effects on cell viability

Using the MTT assay, the cell viability of both Caco-2 and CL-14 cultures infected at MOI 1 or 10 measured 24 h p.i. was similar to mock-infected cultures (fig. 2B). The viability was significantly lowered 48 and 72 h p.i. in cultures infected at MOI 10 and 1, respectively. The maximum decrease in cell viability was achieved 96 h p.i. However, at least 35% cell viability was recorded even in cultures infected at MOI 10, and this did not decrease any further (fig. 2B).

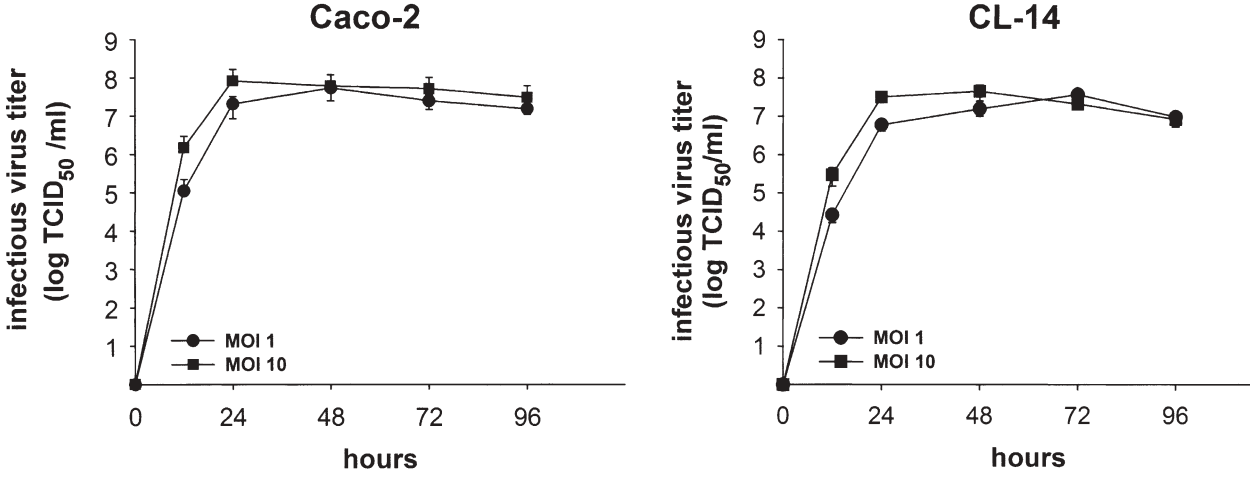

Figure 1. Production of infectious virus titers in Caco-2 cells (*A*) and CL-14 cells (*B*) infected with SARS-CoV FFM-1 strain (MOI 1 and 10) at different time points p.i. Values represent the mean (± SD) from three independent experiments.

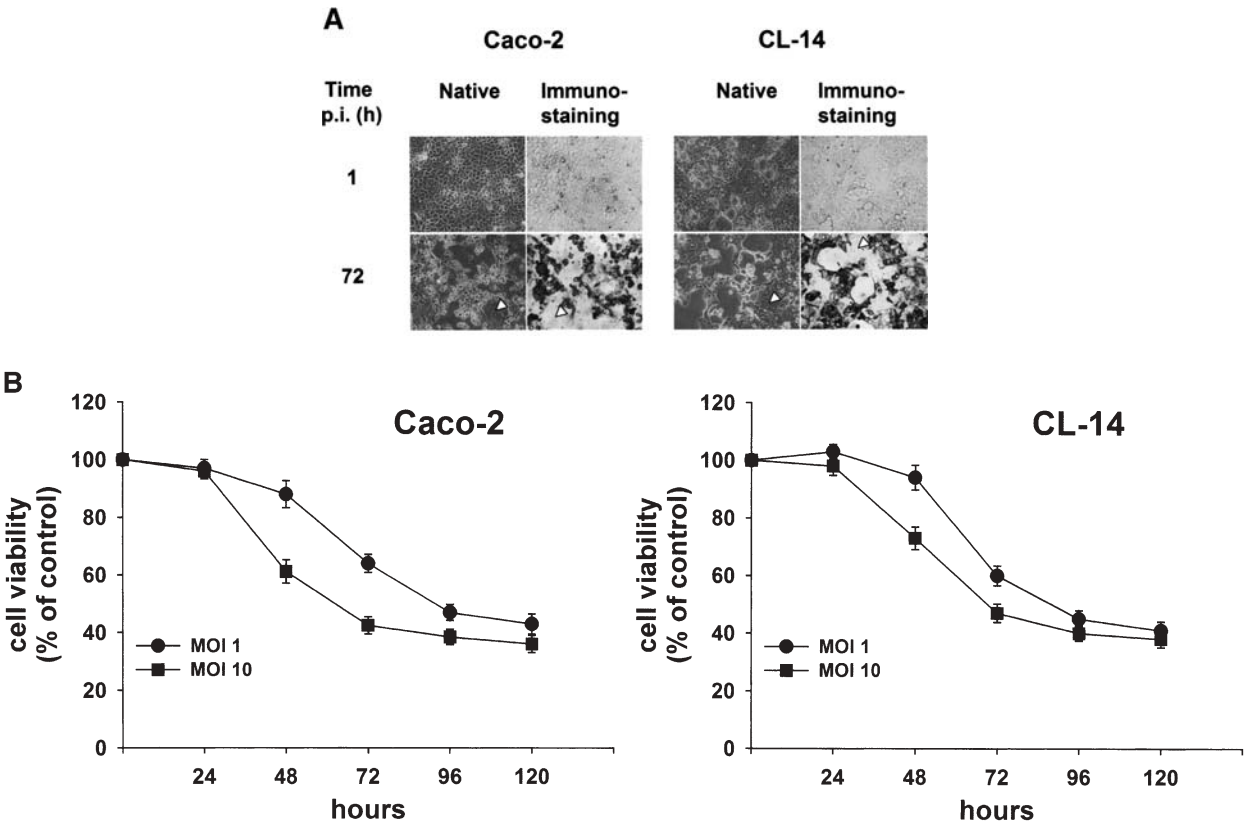

Figure 2. Development of CPE and staining for viral antigens (*A*) and viability (*B*) of Caco-2 and CL-14 cell cultures infected with the SARS-CoV FFM-1 strain at different time points p.i. Results of MTT assay, expressed as percentage of mock-infected control. Values represent the mean (± SD) from three independent experiments. 72 hours post infection some cells adhered to the culture vessel surface and did not stain with immune serum (arrowheads).

SARS-CoV receptor studies

Since ACE2 was identified as a functional SARS-CoV receptor in different cell types [3] we measured whether its expression may correlate with the sensitivity of intestinal cell lines to SARS-CoV infection. Caco-2 and CL-14 expressed ACE2 mRNA and protein which were not detectable in the other cell lines tested (fig. 3A, B). Pre-treatment of both Caco-2 and CL-14 cells with anti-ACE2 antibody reduced at least 20-fold the numbers of SARS-CoV-infected cells, while ACE1 antibody used as control had no effects on numbers of infected cells (fig. 3C).

Ultrastructural study

Caco-2 cell cultures 24 h p.i. consisted of mostly poorly differentiated cells (fig. 4A, B) but also some well-differentiated (villus) enterocytes (fig. 4D). Coronavirus particles were found in both, with more than 30% of cells found to be infected. Viral particles were observed intracellularly within dilated cytoplasmic vesicles (fig. 4C) consistent with dilated endoplasmic reticulum but not in nuclei, and extracellularly both attached to the cytoplasmic membrane and detached from the cells (fig. 4B, E).

Effects on cellular gene expression

The relative abundance of specific mRNA in SARS-CoV-infected cells was compared to mock-infected confluent Caco-2 cell cultures (same passage and identical culture conditions) 24 h p.i. when cell viabilities were similar (fig. 2B). All gene expression experiments were done in duplicate and only genes which were up- or down-regulated in both samples underwent further evaluation. After applying strong restrictions as described in Materials and Methods, resulting genes were grouped according to their function (table1).

We focussed on genes related to apoptosis, chemokines, interferon-induced genes and transcription factors, since these gene groups may play an important role in the pathogenesis of SARS. Expression of the selected genes was confirmed by RT-PCR (fig. 5). In the infected cells, we found an up-regulation of some anti-apoptotic genes including Bcl-2 (only in Caco-2 but not in CL-14 cells) and A20, while several pro-apoptotic genes including Bid, Bad, caspase-2 and caspase-6 were down-regulated. On the other hand, the anti-apoptotic programmed cell death 4 gene (PDCD4) was down-regulated in infected cells. Increased levels of mRNA of members of the AP-1 family of cellular transcription factors including c-jun

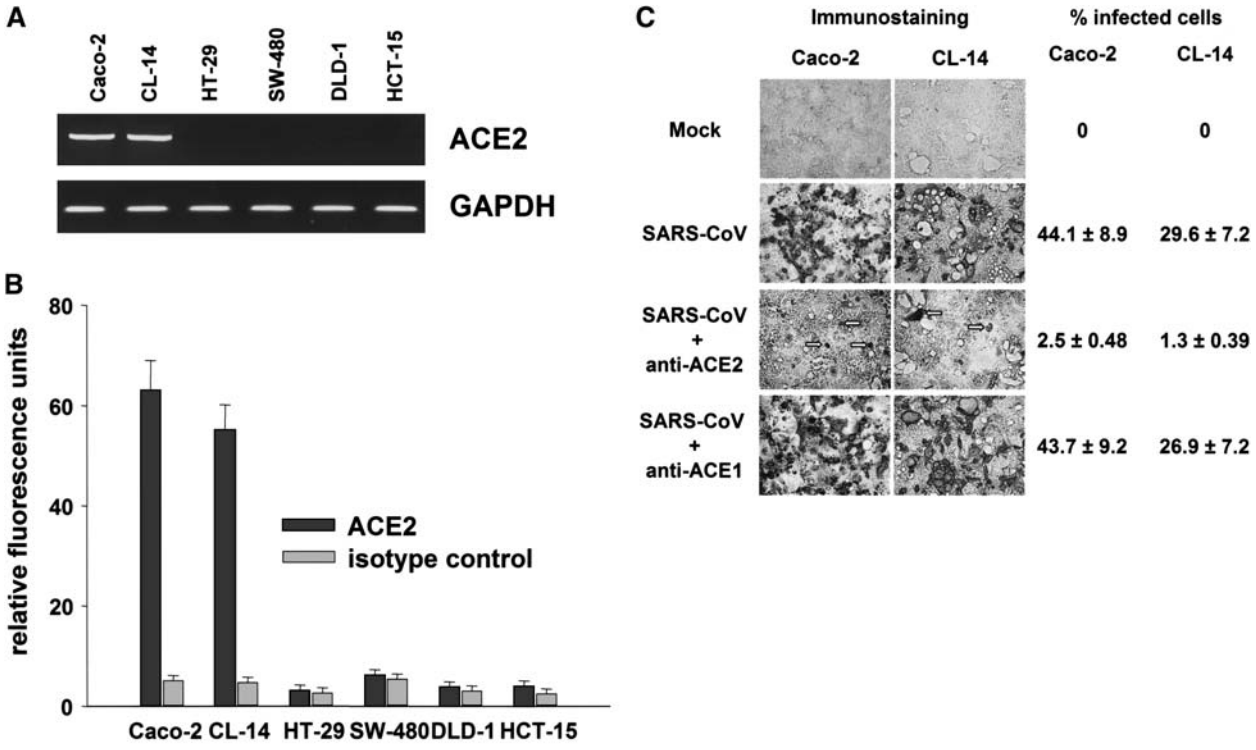

Figure 3. Expression of ACE2 mRNA (*A*) and surface protein (*B*) on Caco-2 and CL-14 cells as well as blocking of SARS-CoV infection by anti-ACE2 antibody (*C*). mRNA was measured by means of RT-PCR and amplification products of ACE2 and GAPDH were visualized with ethidium bromide on an agarose gel. ACE2 surface expression was measured by flow cytometry. Blocking experiments were performed by treatment of cells 60 min before infection with the FFM-1 strain (MOI 1) using goat antibody directed against ACE2 or control antibody directed against ACE1. The data are means (± SD) from three independent experiments.

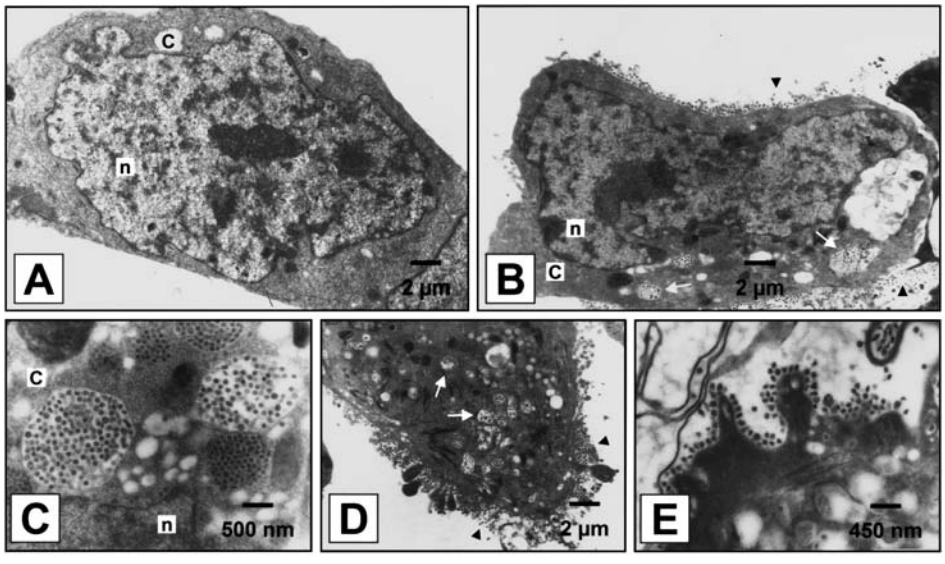

Figure 4. Ultrastructural appearance of mock-infected (*A*) and SARS-CoV-infected (*B*–*E*) Caco-2 cells. A poorly differentiated cell shows viral particles in dilated cytoplasmic vesicles (arrow; *B* and *C*) as well as extracellularly (arrowheads; *B*). A well-differentiated (villus) enterocyte shows viral particles in cytoplasmic vesicles (arrows) and on the cell surface (arrowheads; *D*). Some viral particles attach onto the microvilli, whereas some detach from the cell surface (*E*). c, cytoplasm; n, nucleus.

Table 1. Genes differentially expressed at least threefold in SARS-infected CaCo-2 cells 24 h p.i. compared to mock-infected cells.

Accession No.	Gene	Map	Description
Up-regulation			
Chemokines/cytokines/receptors			
NM_001146	ANGPT1	8q22.3-q23	angiopoietin 1
NM_001200.1	BMP2	20p12	bone morphogenetic protein 2
NM_001201.1	BMP3	4p14-q21	bone morphogenetic protein 3
NM_004591.1	CCL20	2q33-q37	chemokine (C-C motif) ligand 20
NM_002090.1	CCL3	17q11-q21	chemokine (C-C motif) ligand 3
NM_001511.1	CXCL1	4q21	chemokine (C-X-C motif) ligand 1
M57731.1	CXCL2	4q21	chemokine (C-X-C motif) ligand 2
NM_002620.1	CXCL3	4q21	chemokine (C-X-C motif) ligand 3
NM_000584.1	CXCL8	4q13-q21	chemokine (C-X-C motif) ligand 8
NM_001565.1	CXCL10	4q21	chemokine (C-X-C motif) ligand 10
AF030514.1	CXCL11	4q21.2	chemokine (C-X-C motif) ligand 11
NM_002009.1	FGF7	15q15-q21.1	fibroblast growth factor 7 (keratinocyte growth factor)
BG389073	GDF11	12q13.13	growth differentiation factor 11
NM_014440.1	IL1F6	2q12-q14.1	interleukin 1 family, member 6 (epsilon)
NM_000418.1	IL4R	16p11.2-12.1	interleukin 4 receptor
NM_002608.1	PDGFB	22q13.1	platelet-derived growth factor beta polypeptide
NM_002620.1	PF4V1	4q12-q21	platelet factor 4 variant 1
M19154.1	TGFB2	1q41	transforming growth factor, beta 2
Cell cycle			
S67788.1	APC	5q21-q22	adenomatosis polyposis coli
AI421559	RALGDS	9q34.3	ral guanine nucleotide dissociation stimulator
NM_002923	RGS2	1q31	regulator of G-protein signalling 2, 24 kDa
Apoptosis			
AF086790.1	ACON		aconitase precursor
NM_000633.1	BCL2	18q21.3	B cell CLL/lymphoma 2
NM_006561.1	CUGBP2	10p13	CUG triplet repeat, RNA-binding protein 2
NM_017523.1	HSXIAPAF1	17p13.2	XIAP-associated factor-1
AI078167	NFKBIA	14q13	NfκB light polypeptide gene enhancer in B cells inhibitor α
NM_000315.1	PTH	11p15.3-p15.1	parathyroid hormone
NM_006290	A20(TNFAIP3)	6q23	tumour necrosis factor, alpha-induced protein 3
Differentiation			
NM_000348.1	SRD5A2	2p23	steroid-5-alpha-reductase
NM_005725	TSPAN-2	1p12	tetraspan 2
Signal transduction			
D32201	ADRA1A	8p21-p11.2	adrenergic, alpha-1A-, receptor
NM_004041.2	ARRB1	11q13	arrestin, beta 1
L24959	CAMK4	5q21.3	calcium/calmodulin-dependent protein kinase IV
NM_014421.1	DKK2	4q25	dickkopf homologue 2 (*Xenopus laevis*)
NM_001365.1	DLG4	17p13.1	discs, large (*Drosophila*) homologue 4
NM_004417.2	DUSP1	5q34	dual specificity phosphatase 1
BC005047.1	DUSP6	12q22-q23	dual specificity phosphatase 6
NM_004431	EPHA2	1p36	EphA2
U35398.1	GPR68	14q31	G protein-coupled receptor 68
NM_014920	ICK	6p12.3-p11.2	intestinal cell kinase
AW338791	IGFALS	16p13.3	IGF-binding protein, acid-labile subunit
NM_003604	IRS4	Xq22.3	insulin receptor substrate 4
BC002844	NFKB2	10q24	NfκB light polypeptide gene enhancer in B cells 2
AA149639	QKI	6q26-27	homologue of mouse quaking QKI
NM_004841	RASAL2	1q24	RAS protein activator-like 2
S59049	RGS1	1q31	regulator of G-protein signalling 1
AI332407	SFRP1	8p12-p11.1	secreted frizzled-related protein 1
U91903.1	SFRP3	2qter	frizzled-related protein
AF036269	SH3GL3	15q24	SH3-domain GRB2-like 3
X52075	SPN	16p11.2	sialophorin (gpL115, leukosialin, CD43)
Transcription			
NM_021570.2	BARX1	9q12	BarH-like homeobox 1
BE675435	COPEB	10p15	core promoter element-binding protein
NM_001964.1	EGR1	5q31.1	early growth response 1
N25429	EIF3S6	8q22-q23	eukaryotic translation initiation factor 3, subunit 6, 48 kDa
BF060791	ETV5	3q28	ets variant gene 5 (ets-related molecule)
NM_002017.2	FLI1	11q24.1-q24.3	Friend leukaemia virus integration 1

Table 1 (continued)

Accession No.	Gene	Map	Description
V01512	FOS	14q24.3	c-fos
NM_001546.1	ID4	6p22-p21	inhibitor of DNA-binding 4,
J04111	JUN	1p32-p31	c-jun
NM_000475.2	NR0B1	Xp21.3-p21.2	nuclear receptor subfamily 0, group B, member 1
NM_002616.1	PER1	17p13.1-17p12	period homologue 1 (*Drosophila*)
BC005325.1	SSX4	Xp11.23	synovial sarcoma, X breakpoint 4
NM_030751.1	TCF8	10p11.2	transcription factor 8 (represses interleukin 2 expression)
BC004145.1	TNRC4	1q21	trinucleotide repeat-containing 4
NM_014112.1	TRPS1	8q24.12	trichorhinophalangeal syndrome 1
NM_000551.1	VHL	3p26-p25	von Hippel-Lindau syndrome
NM_013256.1	ZNF180	19q13.2	zinc finger protein 180 (HHZ168)
NM_006448.1	ZNF384		zinc finger protein 384
Protein folding			
AF007162	CRYAB	11q22.3-q23.1	crystallin, alpha B
AF052173	TBCD	17q25.3	tubulin-specific chaperone d
DNA recombination			
NM_004507	HUS1	7p13-p12	HUS1 checkpoint homologue
Metabolism			
AF182276.1	CYP2E1	10q24.3-qter	cytochrome P450, family 2, subfamily E, polypeptide 1
NM_005021.1	ENPP3	6q22	ectonucleotide pyrophosphatase/phosphodiesterase 3
NM_005110.1	GFPT2	5q34-q35	glutamine-fructose-6-phosphate transaminase 2
AL527430	GSTM3	1p13.3	glutathione S-transferase M3 (brain)
AU121975	PAICS	4pter-q21	phosphoribosylaminoimidazole carboxylase
NM_000329.1	RPE65	1p31	retinal pigment epithelium-specific protein 65 kDa
Interferon-induced genes			
NM_005101.1	G1P2	1p36.33	interferon, alpha-inducible protein (clone IFI-15K)
NM_022873.1	G1P3	1p35	interferon, alpha-inducible protein (clone IFI-6-16)
NM_006417.1	IFI44	1p31.1	interferon-induced protein 44
NM_001548.1	IFIT1	10q25-q26	interferon-induced protein with tetratricopeptide repeats 1
NM_001549.1	IFIT4	204747_at	interferon-induced protein with tetratricopeptide repeats 4
NM_003641.1	IFITM1	11p15.5	interferon induced transmembrane protein 1 (9-27)
NM_006435.1	IFITM2	11p15.5	interferon induced transmembrane protein 2 (1-8D)
NM_004030.1	IRF7	11p15.5	interferon regulatory factor 7
NM_005101	ISG15	1p36.33	interferon-stimulated protein, 15 kDa
NM_002462.1	MxA	21q22.3	interferon-inducible protein p78
NM_016817.1	OAS2	12q24.2	2′-5′-oligoadenylate synthetase 2, 69/71 kDa
NM_003733.1	OASL	12q24.2	2′-5′-oligoadenylate synthetase-like
Miscellaneous genes			
NM_000443.2	ABCB4	7q21.1	ATP-binding cassette, sub-family B (MDR/TAP), member 4
NM_000706.2	AVPR1A	12q14-q15	arginine vasopressin receptor 1A
NM_016279.1	CDH9	5p14	cadherin 9, type 2 (T1-cadherin)
NM_004397.2	DDX6	11q23.3	DEAD (Asp-Glu-Ala-Asp) box polypeptide 6
AK022087.1	DES	2q35	desmin
U56236.1	FCAR	19q13.2-q13.4	Fc fragment of IgA
NM_006682	FGL2	7q11.23	fibrinogen-like 2
NM_005204.1	MAP3K8	10p12.1	mitogen-activated protein kinase kinase kinase 8
NM_005952.1	MT1X	16q13	metallothionein 1X
NM_014314.1	RIG-I	9p12	DEAD/H (Asp-Glu-Ala-Asp/His) box polypeptide
NM_014139.1	SCN11A	3p24-p21	sodium channel, voltage-gated, type XI, alpha
NM_003095.1	SNRPF	12q23.1	small nuclear ribonucleoprotein polypeptide F
NM_000593.2	TAP1	6q21.3	transporter 1, ATP-binding cassette, sub-family B
(MDR/TAP)AL574096	TFPI2	7q22	tissue factor pathway inhibitor 2
AA813018	TJP1	15q13	tight junction protein 1 (zona occludens 1)
Down-regulation			
Chemokines/cytokines/receptors			
M60459	EPOR	19p13.3-p13.2	erythropoietin receptor
NM_000121	EPOR		erythropoietin receptor precursor
NM_001562.1	IL18	11q22.2-q22.3	interleukin 18 (interferon gamma-inducing factor)
NM_002415.1	MIF	22q11.23	macrophage migration inhibitory factor
Cell cycle			
NM_002012.1	FHIT	3p14.2	fragile histidine triad gene
NM_005256.1	GAS2	11p14.3-15.2	growth arrest-specific 2

Table 1 (continued)

Accession No.	Gene	Map	Description
NM_005862.1	STAG1	3q22.2	stromal antigen 1
BG034328	TFDP2	3q23	transcription factor Dp-2 (E2F dimerization partner 2)
Apoptosis			
U66879	BAD	11q12.3	BCL2-antagonist of cell death
NM_001196.1	BID	22q11.1	BH3 interacting domain death agonist
NM_001224.1	CASP2	7q34-q35	caspase 2, apoptosis-related cysteine protease
U20537.1	CASP6	4q25	caspase 6, apoptosis-related cysteine protease
NM_014430.1	CIDEB	14q11.2	cell death-inducing DFFA-like effector
BC005299.1	CYCS	7p15.2	cytochrome c, somatic
AA485440	SPHK2	19q13.3	sphingosine kinase 2
M55983.1	DNASE1	16p13.3	deoxyribonuclease
AK024029.1	MOAP1	14q32	modulator of apoptosis 1
NM_014456.	PDCD4	10q24	programmed cell death 4 (neoplastic transformation inhibitor)
NM_006281.1	STK3	8q22.1	serine/threonine kinase 3 (STE20 homologue, yeast)
Signal transduction			
NM_001177.2	ARL1	12q23.3	ADP-ribosylation factor-like 1
NM_005308.1	GPRK5	10q24-qter	G protein-coupled receptor kinase 5
AL570294	HRMT1L1	21q22.3	HMT1 hnRNP methyltransferase-like
U50748.1	LEPR	1p31	leptin receptor
NM_021183.1	LOC57826	Xq25	hypothetical protein similar to small G proteins, especially RAP-2A
NM_002757.1	MAP2K5	15q22.2	mitogen-activated protein kinase kinase 5
AW195581	MCLC	1p13.2	Mid-1-related chloride channel 1
BF001665	OGT	Xq13	O-linked N-acetylglucosamine (GlcNAc) transferase
NM_005884.2	PAK4	19q13.13	p21(CDKN1A)-activated kinase 4
AL574319	PDK2	17q21.32	pyruvate dehydrogenase kinase, isoenzyme 2
AI189609	RAB2	8q12.1	RAB2, member RAS oncogene family
AF125393.1	RAB27A	15q15-q21.1	RAB27A, member RAS oncogene family
BG338251	RAB7L1	1q32	RAB7, member RAS oncogene family-like 1
AB018283.2	RHOBTB1	10q21.2	Rho-related BTB domain-containing 1
AB014486.1	SCAP2	7p21-p15	src family-associated phosphoprotein 2
NM_003025.1	SH3GL1	19p13.3	SH3-domain GRB2-like 1
NM_013381.1	TRHDE	12q15-q21	thyrotropin-releasing hormone-degrading ectoenzyme
Protein folding			
NM_003796	C19orf2	19q12	chromosome 19 open reading frame 2
NM_016074.1	CGI-143	1p36.13-q31.3	CGI-143 protein
AF109161.1	CITED2	6q23.3	Cbp/p300-interacting transactivator
BC005250.1	CRSP9	5q33.3	cofactor required for Sp1 transcriptional activation
NM_017946	FKBP14	7p15.1	FK506 binding protein 14, 22 kDa
AI935162	HPIP	1q21.3	haematopoietic PBX-interacting protein
NM_020347.1	LZTFL1	3p21.3	leucine zipper transcription factor-like 1
NM_005360.2	MAF	16q22-q23	v-maf musculoaponeurotic fibrosarcoma oncogene homologue
AA421957	MED8	1p34.1	mediator of RNA polymerase II transcription
AV756536	MLLT3	9p22	myeloid/lymphoid or mixed-lineage leukaemia
AB028973.1	MYT1	20q13.33	myelin transcription factor 1
L20433.1	POU4F1	13q21.1-q22	POU domain, class 4, transcription factor 1
AW027312	RFX5	1q21	regulatory factor X, 5 (influences HLA class II expression)
BC000519.1	RUVBL1	3q21	RuvB-like 1
NM_003113.1	SP100	2q37.1	nuclear antigen Sp100
BC002802.1	SUPT4H1	17q21-q23	suppressor of Ty 4 homologue 1
AA081084	TAZ	3q23-q24	transcriptional coactivator with PDZ-binding motif (TAZ)
NM_003447.1	ZNF165	6p21.3	zinc finger protein 165
Metabolism			
NM_001086.1	AADAC	3q21.3-q25.2	arylacetamide deacetylase (esterase)
AI653169	AK3	1p31.3	adenylate kinase 3
U05598.1	AKR1C2	10p15-p14	aldo-keto reductase family 1, member C2
NM_002108.2	AKR1D1	7q32-q33	aldo-keto reductase family 1, member D1
BC000977.1	ALAD	9q34	aminolevulinate, delta-, dehydratase
NM_000694.1	ALDH3B1	11q13	aldehyde dehydrogenase 3 family, member B1
AU149534	ALDH7A1	5q31	aldehyde dehydrogenase 7 family, member A1
NM_005165.1	ALDOC	17cen-q12	aldolase C, fructose-bisphosphate
NM_001150.1	ANPEP	15q25-q26	alanyl (membrane) aminopeptidase
AF161454.1	APOM	6p21.31	apolipoprotein M

Table 1 (continued)

Accession No.	Gene	Map	Description
NM_000049.1	ASPA	17pter-p13	aspartoacylase (aminoacylase 2, Canavan disease)
NM_000709.1	BCKDHA	19q13.1-q13.2	branched-chain keto acid dehydrogenase E1
AY028632.1	CAT	11p13	catalase
AL568982	CDS2	20p13	CDP-diacylglycerol synthase
AA723370	CGI-105	2p24.3-p11.2	CGI-105 protein
AF154830.1	CPS1	2q35	carbamoyl-phosphate synthetase 1, mitochondrial
BF001714	CPT1A	11q13.1-q13.2	carnitine palmitoyltransferase 1A (liver)
NM_000098.1	CPT2	1p32	carnitine palmitoyltransferase II
AL354872	CTH	1p31.1	cystathionase (cystathionine gamma-lyase)
AJ222967	CTNS	17p13	cystinosis, nephropathic
NM_018973.1	DPM3	1q21.3	dolichyl-phosphate mannosyltransferase polypeptide 3
NM_000120.2	EPHX1	1q42.1	epoxide hydrolase 1, microsomal (xenobiotic)
AF233336.1	EPHX2	8p21-p12	epoxide hydrolase 2, (cytoplasmic)
NM_020973.1	GBA3	4p15.31	glucosidase, beta, acid 3 (cytosolic)
AW299507	GGPS1	1q43	geranylgeranyl diphosphate synthase 1
X62078	GM2A	5q31.3-q33.1	GM2 ganglioside activator protein
NM_016576.1	GMPR2	14q11.2	guanosine monophosphate reductase 2
NM_000862.1	GSTM1	1p13.3	glutathione S-transferase M1
BC001453.1	GSTZ1	14q24.3	glutathione transferase zeta 1 (maleylacetoacetate isomerase)
NM_005326.1	HAGH	16p13.3	hydroxyacyl glutathione hydrolase
NM_002108.2	HAL	12q22-q24.1	histidine ammonia-lyase
NM_000191.1	HMGCL	1p36.1-p35	3-hydroxymethyl-3-methylglutaryl-coenzyme A lyase
NM_000862.1	HSD3B1	1p13.1	hydroxy-delta-5-steroid dehydrogenase
D55639.1	KYNU	2q22.1	kynureninase (L-kynurenine hydrolase)
NM_020379.1	MAN1C1	1p35	mannosidase, alpha, class 1C, member 1
NM_000898.1	MAOB	Xp11.4-p11.3	monoamine oxidase B
AI039874	NQO1	16q22.1	NAD(P)H dehydrogenase, quinone 1
AL574319	PDK2	17q21.32	pyruvate dehydrogenase kinase, isoenzyme 2
NM_016134.1	PGCP	8q22.2	plasma glutamate carboxypeptidase
AK021676.1	PGM3	6q14.1-q15	phosphoglucomutase 3
NM_002676.1	PMM1	22q13.2	phosphomannomutase 1
BC005989.1	PNLIPRP2	10q26.11	pancreatic lipase-related protein 2
NM_022128.1	RBSK	2p23.3	ribokinase
AW190316	SHMT2	12q12-q14	serine hydroxymethyltransferase 2 (mitochondrial)
NM_000340.1	SLC2A2	3q26.1-q26.2	solute carrier family 2 (facilitated glucose transporter), member 2
AF059203.1	SOAT2	12q13.13	sterol O-acyltransferase 2
NM_003167.1	SULT2A1	19q13.3	sulphotransferase family, cytosolic, 2A member 1
BE895437	TK2	16q22-q23.1	thymidine kinase 2, mitochondrial
NM_001076.1	UGT2B15	4q13	UDP glycosyltransferase 2 family, polypeptide B15
NM_001077.1	UGT2B17	4q13	UDP glycosyltransferase 2 family, polypeptide B17
AF177272.1	UGT2B28	4q13.3	UDP glycosyltransferase 2 family, polypeptide B28
NM_016327.1	UPB1	22q11.2	ureidopropionase, beta
M14016.1	UROD	1p34	uroporphyrinogen decarboxylase
DNA repair			
NM_007195.1	POLI	18q21.1	polymerase (DNA directed) iota
NM_005053	RAD23A	19p13.2	RAD23 homolog A
NM_002907.1	RECQL	12p12	RecQ protein-like (DNA helicase Q1-like)
NM_014311.1	SMUG1	12q13.11	single-strand selective monofunctional uracil DNA glycosylase
NM_000380.1	XPA	9q22.3	xeroderma pigmentosum, complementation group A
RNA processing			
NM_030934	C1orf25	1q25.2	chromosome 1 open reading frame 25
NM_014953	DIS3	13q21.32	mitotic control protein dis3 homologue
NM_006567	FARS1	6p25.1	phenylalanine-tRNA synthetase
NM_006867	RBPMS	8p12-p11	RNA-binding protein with multiple splicing
Proliferation			
NM_013407.1	DHPS	19p13.11	deoxyhypusine synthase
NM_000508.2	FGA	4q28	fibrinogen, A alpha polypeptide
NM_001481.1	GAS8	16q24.3	growth arrest-specific 8
NM_005537.1	ING1	13q34	inhibitor of growth family, member 1
NM_002888.1	RARRES1	3q25.32	retinoic acid receptor responder (tazarotene induced) 1
NM_006443.1	RCL	6p21.1	putative c-Myc-responsive
NM_005981.1	SAS	12q13.3	sarcoma-amplified sequence
Miscellaneous genes			
NM_004306	ANXA13	8q24.1-q24.2	annexin A13

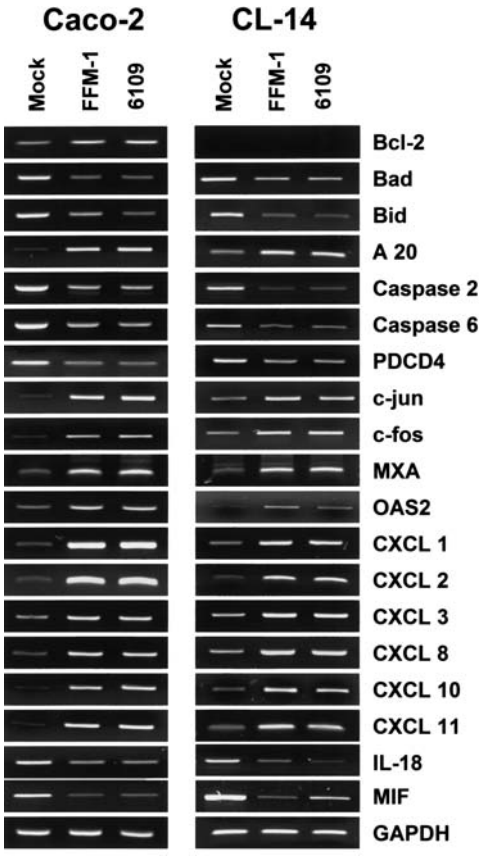

Figure 5. Validation of microarray data with semiquantitative RT-PCR. Transcripts from one housekeeping gene (GAPDH) and 19 other cellular genes were assessed for their relative abundance in mock-infected and SARS-infected (strains FFM-1 and 6109) colon carcinoma cell lines (Caco-1 and CL-14). All genes showed a pattern of transcript abundance consistent with the microarray data.

and c-fos were observed in the infected cells. Concerning cytokine/chemokine-related genes, our results showed an up-regulation of several CXC chemokines; among the down-regulated genes we found interleukin (IL)-18 and macrophage migration inhibitory factor (MIF). Several interferon-induced genes were up-regulated, including the human 2′-5′ oligoadenylate synthetase 2 gene (OAS2) and human myxovirus resistance-1 gene (MXA). SARS-CoV strains FFM-1 and 6109 influenced similarly the expression of the selected genes (fig. 5). Neither UV-inactivated virus nor virus-free filtered cell culture supernatants caused any changes in gene expression pattern compared to mock-infected cells (data not shown).

Discussion

To provide an experimental model for the study of SARS gastrointestinal pathology, we tested the sensitivity of six intestinal cell lines to SARS-CoV infection. In addition to Caco-2 cells which were previously shown to be permissive to SARS-CoV [8], only CL-14 cells promoted SARS-CoV replication. CL-14 cells show features of well-differentiated enterocytes [14] while Caco-2 cells show an undifferentiated phenotype with the ability to undergo spontaneous enterocytic differentiation after reaching confluence [15]. We infected Caco-2 cells 2–3 days after confluence, i.e. when electron microscopy identified mostly poorly differentiated enterocytes and only few well-differentiated (villus) enterocytes. Both poorly and well-differentiated enterocytes supported SARS-CoV replication suggesting that the sensitivity of intestinal epithelial cells does not depend on a particular stage of cellular differentiation.

ACE2 has recently been shown to be a functional receptor for SARS-CoV [3] and surface ACE2 is abundantly present on enterocytes of the small intestine [16]. The present study indicates that cell surface expression of ACE2 appears to be essential for infection of intestinal cells. Depending on the MOI used, CL-14 and Caco-2 cells produced maximum infectious virus titres 48–72 h p.i., at times when few effects on cell viability and CPE were observed. Later, i.e. 72 and 96 h p.i., cell viability was markedly decreased without a concomitant further increase of virus titres. Although some cells that survived virus infection even in cultures infected at MOI 10 for 96 h did not stain with immune serum, we did not succeed in sub-cultivation of surviving cells. Whether or not these cells are infected and whether expression of viral antigens is below the detection limit of the method used is not clear at present.

Gene expression analysis performed 24 h p.i. demonstrated that SARS-CoV infection influences expression of several cellular genes which may be important for SARS intestinal pathogenesis. For example, SARS-CoV up-regulated anti-apoptotic genes such as Bcl-2 and A20 while it down-regulated pro-apoptotic genes such as Bid, Bad, caspase-2 and caspase-6. In a murine model, Bcl-2 overexpression in gut epithelial cells, decreased the apoptosis [17] and protected against intestinal injury [18]. Although Bcl-2 was detectable only in Caco-2 cells, other regulators of the apoptotic mitochondrial pathway including pro-apoptotic Bcl-2 homologues Bid and Bad were down-regulated by SARS-CoV in both Caco-2 and CL-14 cells. Since Bid and Bad are involved in the regulation of intestinal epithelial cell survival [19], their role in SARS-CoV intestinal infection should be studied further. In both cell lines, SARS-CoV up-regulated A20 which may protect different cell types against tumour necrosis factor (TNF)-mediated programmed cell death and is critical for limiting inflammation by terminating TNF-induced nuclear factor (NF)-κB responses in the intestine and other organs [20]. In addition, down-regulation of caspase-2 and caspase-6 in infected intestinal cell lines may be of interest as these caspases were shown to be important mediators of apoptosis in gastrointestinal

epithelium [21, 22]. The results show that SARS-CoV-infected epithelial cells develop an anti-apoptotic response which may be important to inhibit or delay destruction of infected enterocytes. These findings are consistent with clinical observations demonstrating a relatively normal endoscopic and microscopic appearance of the intestine in patients with SARS [5].

On the other hand, SARS-CoV suppressed expression of the anti-apoptotic gene PDCD4 which is constitutively expressed in most normal tissues including lung and intestine [23]. Apart from its effects in the regulation of apoptosis, PDCD4 was shown to play a role in inhibition of translation by direct interaction with eukaryotic translation initiation factor 4A (eIF4A) [23, 24]. This finding is of interest since activity of eIF4E (together with eIF4A and eIF4G forming the translation initiation factor complex eIF4F) was shown to be important for replication of murine coronavirus [25]. Moreover, PDCD4 has the ability to suppress transactivation of activator protein (AP)-1 [23]. Since the SARS-CoV nucleocapsid was shown to activate the AP-1 transduction pathway [26], it will be of interest to show whether there may be a mechanistic link between PDCD4 suppression and enhancement of AP-1 tranactivation in SARS-CoV-infected cells. The present observations demonstrate that SARS-CoV infection elevated mRNA levels of AP-1 subunits c-Fos and c-Jun in intestinal cells which could also increase AP-1 transactivation.

Infection with most viruses up-regulates different interferon (IFN)-induced genes which may establish an anti-viral state within cells. Its major effectors and indicators include double-stranded RNA-dependent protein kinase (PKR), OAS and MX proteins [27]. SARS-CoV infection of Caco-2 cells up-regulated OAS2 and MXA but not PKR genes. The discrepancy between transcriptional activation of IFN-induced genes and the ability of SARS-CoV to replicate in Caco-2 cells could be explained by the existence of a specific viral mechanism for escaping IFN-induced anti-viral effects common to most viruses [28]. The enteropathogenic potential of HCoV-OC43 (strain Paris) has been suggested to be due to its inability to induce IFN-α [29]. Recently, we showed that IFN-α and IFN-β (type I IFN) inhibited SARS-CoV replication in Caco-2 cells while IFN-γ (type II IFN) was not effective [8]. Moreover, IFN-β was 50–90 times more potent than IFN-α against different SARS-CoV strains. The differences in anti-viral activity of different types of IFN could result from their ability to differentially influence expression of cellular genes important for anti-viral activity. For example, treatment of the human fibrosarcoma cell line HT1080 (expressing both type I and type II IFN receptors) with IFN-β stimulated PKR which was not stimulated by IFN-α or IFN-γ [30]. Since PKR was not up-regulated in the infected Caco-2 cells and virus replication progressed despite up-regulation of OAS2 and MXA, a role for PKR in SARS-CoV replication must be elucidated.

Although enteric pathogens such as viruses, protozoans, multicellular helminths and enteroinvasive bacteria vary in their mode of infection, enterocytes display a common chemokine/cytokine profile in response to infection. Several ELR+CXC chemokines (containing a conserved glutamate-leucine-arginine sequence) including CXCL1 (groα), CXCL2 (groβ), CXCL3 (groγ) and CXCL8 (IL-8) were up-regulated in SARS-CoV infected Caco-2 cells. These chemokines mainly regulate neutrophil trafficking [31]. In addition, SARS-CoV induced in Caco-2 cells non-ELR CXC chemokines CXCL10/IFN-γ inducible protein-10 (IP-10) and CXCL11/IFN-inducible T cell alpha chemoattractant (I-TAC) which are potent CD4+ T cell chemoattractants [32, 33]. Rotavirus infection was shown to induce CXCL1, CXCL8 and CXCL10 in intestinal cell lines [34]. Mucosal inflammation associated with rotavirus infection is predominantly mononuclear, i.e. consists of monocytes and T lymphocytes [35], although neutrophil infiltration is found in some cases [34]. In contrast, biopsy specimens taken from the colon and terminal ileum of patients with SARS failed to demonstrate any inflammatory infiltrates [5]. Neutrophil infiltration in the intestine of SARS patients may be limited despite neutrophilia due to changes of cytokine/chemokine levels in the intestinal environment. We observed that SARS-CoV infection of Caco-2 cells inhibited expression of IL-18 which is constitutively expressed in intestinal epithelial cells [36]. Suppression of IL-18 levels reduces neutrophil accumulation in liver and lungs [37]. The absence of T lymphocyte infiltration of the intestine in SARS may be a consequence of the profound decline of both CD4+ and CD8+ lymphocytes in the blood [38], possibly resulting from lymphocyte apoptosis [39]. Although macrophage counts were increased in lungs [40], macrophage infiltration was absent from the gut of SARS patients [5]. In Caco-2 cells, SARS-CoV down-regulated MIF. Recently, MIF was identified as a major factor produced by intestinal cells in response to microbial infection regulating macrophage emigration, inflammation and cell metabolism [41].

Some of the chemokines we found up- or down-regulated in vitro were also changed in serum samples from SARS patients. For example, serum levels of CXCL10 and IL-8 were increased whereas IL-18 was decreased [42, 43]. This justifies the use of intestinal cell lines as a model to study the direct effects of SARS-CoV infection on gene expression in permissive human cells. Given the intestinal tropism of SARS-CoV, the results presented here provide several important hints at possible mechanisms of intestinal pathogenesis and potential novel therapeutic targets in SARS.

Acknowledgements. The authors wish to acknowledge valuable technical support by G. Meincke, L. Stegmann and C. Sippel. The authors are grateful to H. Kabickova for transmission electron microscopy experiments.

1 Drosten C., Guenther S., Preiser W., Werf S. van der, Brodt H. R., Becker S. et al. (2003) Identification of a novel coronavirus in patients with severe acute respiratory syndrome. N. Engl. J. Med. **348:** 1967–1976
2 Fowler R. A., Lapinsky S. E., Hallett D., Detsky A. S., Sibbald W. J., Slutsky A. S. et al. (2003) Critically ill patients with severe acute respiratory syndrome. JAMA **290:** 367–373
3 Li W., Moore M. J., Vasilieva N., Sui J., Wong S. K., Berne M. A. et al. (2003) Angiotensin-converting enzyme 2 is a functional receptor for the SARS coronavirus. Nature **426:** 450–454
4 Peiris J. S., Chu C. M., Cheng V. C., Chan K. S., Hung I. F., Poon L. L. et al. (2003) Clinical progression and viral load in a community outbreak of coronavirus-associated SARS pneumonia: a prospective study. Lancet **361:** 1767–1772
5 Leung W. K., To K. F., Chan P. K., Chan H. L., Wu A. K., Lee N. et al. (2003) Enteric involvement of severe acute respiratory syndrome-associated coronavirus infection. Gastroenterology **125:** 1011–1017
6 Booth C. M., Matukas L. M., Tomlinson G. A., Rachlis A. R., Rose D. B., Dwosh H. A. et al. (2003) Clinical features and short-term outcomes of 144 patients with SARS in the greater Toronto area. JAMA **289:** 2801–2809
7 Cheng V. C., Hung I. F., Tang B. S., Chu C. M., Wong M. M., Chan K. H. et al. (2004) Viral replication in the nasopharynx is associated with diarrhea in patients with severe acute respiratory syndrome. Clin. Infect. Dis. **38:** 467–475
8 Cinatl J. Jr., Morgenstern B., Bauer G., Chandra P., Rabenau H. and Doerr H. W. (2003) Treatment of SARS with human interferons. Lancet **362:** 293–294
9 Cinatl J. Jr., Morgenstern B., Bauer G., Chandra P., Rabenau H. and Doerr H. W. (2003) Glycyrrhizin, an active component of liquorice roots, and replication of SARS-associated coronavirus. Lancet **361:** 2045–2046
10 Cinatl J. Jr., Cinatl J., Kotchetkov R., Vogel J.-U., Woodcock B. G., Matousek J. et al. (1999) Bovine seminal ribonuclease selectively kills human multidrug-resistant neuroblastoma cells via induction of apoptosis. Int. J. Oncol. **15:** 1001–1009
11 Brazma A., Hingamp P., Quackenbush J., Sherlock G., Spellman P., Stoeckert C. et al. (2001) Minimum information about a microarray experiment (MIAME) toward standards for microarray data. Nat. Genet. **29:** 365–371
12 Hofmann W. K., Vos S., de Elashoff D., Gschaidmeier H., Hoelzer D., Koeffler H. P. et al. (2002) Relation between resistance of Philadelphia-chromosome-positive acute lymphoblastic leukaemia to the tyrosine kinase inhibitor STI571 and gene-expression profiles: a gene-expression study. Lancet **359:** 481–486
13 Rozen S. and Skaletsky H. (2000) Primer3 on the WWW for general users and for biologist programmers. Methods Mol. Biol. **132:** 365–386
14 Farrell T, Pettengill O, Longneck D., Cate C. and Cohn K. (2000) Growing colorectal tumors: minimizing microbial and stromal competition and assessing in vitro selection pressures. Cytotechnology **34:** 205–211
15 Pinto M., Robine-Leon S., Appay M., Kedinger M., Triadou N., Dussaulx E. et al. (1983) Enterocyte-like differentiation and polarisation of the human colon carcinoma cell line Caco-2 in culture. Biol. Cell **47:** 323–330
16 Hamming I., Timens W., Bulthuis M., Lely A., Navis G. J. and Goor H. van (2004) Tissue distribution of ACE2 protein, the functional receptor for SARS coronavirus: a first step in understanding SARS pathogenesis. J. Pathol. **203:** 631–637
17 Coopersmith C. M., Stromberg P. E., Dunne W. M., Davis C. G., Amiot D. M., Buchman T. G. et al. (2002) Inhibition of intestinal epithelial apoptosis and survival in a murine model of pneumonia-induced sepsis. JAMA **287:** 1716–1721
18 Wildhaber B. E., Yang H. and Teitelbaum D. H. (2003) Total parenteral nutrition-induced apoptosis in mouse intestinal epithelium: modulation by keratinocyte growth factor. J. Surg. Res. **112:** 144–151
19 Gauthier R., Harnois C., Drolet J. F., Reed J. C., Vezina A. and Vachon P. H. (2001) Human intestinal epithelial cell survival: differentiation state-specific control mechanisms. Am. J. Physiol. Cell Physiol. **280:** C1540–C1554
20 Lee E. G., Boone D. L., Chai S., Libby S. L., Chien M., Lodolce J. P. et al. (2000) Failure to regulate TNF-induced NF-kappaB and cell death responses in A20-deficient mice. Science **289:** 2350–2354
21 Tarnawski A. S. and Szabo I. (2001) Apoptosis-programmed cell death and its relevance to gastrointestinal epithelium: survival signal from the matrix. Gastroenterology **120:** 294–299
22 Grossmann J., Artinger M., Grasso A. W., Kung H. J., Scholmerich J., Fiocchi C. et al. (2001) Hierarchical cleavage of focal adhesion kinase by caspases alters signal transduction during apoptosis of intestinal epithelial cells. Gastroenterology **120:** 79–88
23 Lankat-Buttgereit B. and Göke R. (2003) Programmed cell death protein 4 (pdcd4): a novel target for antineoplastic therapy? Biol. Cell **95:** 515–519
24 Yang H. S., Cho M. H., Zakowicz H., Hegamyer G., Sonenberg, N. and Colburn N. H. (2004) A novel function of the MA-3 domains in transformation and translation suppressor Pdcd4 is essential for its binding to eukaryotic translation initiation factor 4A. Mol. Cell Biol. **24:** 3894–3906
25 Banerjee S, Narayanan K, Mizutani T and Makino S (2002) Murine coronavirus replication-induced p38 mitogen-activated protein kinase activation promotes interleukin-6 production and virus replication in cultured cells. J. Virol. **76:** 5937–5948
26 He R., Leeson A., Andonov A., Li Y., Bastien N., Cao J., et al. (2003) Activation of AP-1 signal transduction pathway by SARS coronavirus nucleocapsid protein. Biochem. Biophys. Res. Commun. **311:** 870–876
27 Sen G. C. (2001) Viruses and interferons. Annu. Rev. Microbiol. **55:** 255–281
28 Urosevic N. (2003) Is flavivirus resistance interferon type I-independent? Immunol. Cell Biol. **81:** 224–229
29 Collins A. R. (1990) Comparison of the replication of distinct strains of human coronavirus OC43 in organotypic human colon cells (Caco-2) and mouse intestine. Adv. Exp. Med. Biol. **276:** 497–503
30 Der S. D., Zhou A., Williams B. R. and Silverman R. H. (1998) Identification of genes differentially regulated by interferon alpha, beta, or gamma using oligonucleotide arrays. Proc. Natl. Acad. Sci. USA **95:** 15623–15628
31 Dwinell M. B., Johanesen P. A. and Smith J. M. (2003) Immunobiology of epithelial chemokines in the intestinal mucosa. Surgery **133:** 601–607
32 Loetscher M., Gerber B., Loetscher P., Jones S. A., Piali L., Clark-Lewis I. et al. (1996) Chemokine receptor specific for IP10 and mig: structure, function, and expression in activated T-lymphocytes. J. Exp. Med. **184:** 963–969
33 Cole K. E., Strick C. A., Paradis T. J., Ogborne K. T., Loetscher M., Gladue R. P. et al. (1998) Interferon-inducible T cell alpha chemoattractant (I-TAC): a novel non-ELR CXC chemokine with potent activity on activated T cells through selective high affinity binding to CXCR3. J. Exp. Med. **187:** 2009–2021
34 Casola A., Estes M. K., Crawford S. E., Ogra P. L., Ernst P. B., Garofalo R. P. et al. (1998) Rotavirus infection of cultured intestinal epithelial cells induces secretion of CXC and CC chemokines. Gastroenterology **114:** 947–955
35 Davidson G. P. and Barnes G. L. (1979) Structural and functional abnormalities of the small intestine in infants and young children with rotavirus enteritis. Acta Paediatr Scand **68:** 181–186
36 Pizarro T. T., Michie M. H., Bentz M., Woraratanadharm J., Smith M. F. Jr, Foley E. et al. (1999) IL-18, a novel immunoregulatory cytokine, is up-regulated in Crohn's disease:

expression and localization in intestinal mucosal cells. J. Immunol. **162:** 6829–6835
37 Dinarello C. A. and Fantuzzi G. (2003) Interleukin-18 and host defense against infection. J. Infect. Dis. **187:** S370-S384.
38 Cui W., Fan Y., Wu W., Zhang F., Wang J. Y. and Ni A. P. (2003) Expression of lymphocytes and lymphocyte subsets in patients with severe acute respiratory syndrome. Clin. Infect. Dis. **37:** 857–859
39 O'Donnell R., Tasker R. C. and Roe M. F. E. (2003) SARS: understanding the coronavirus. Apoptosis may explain lymphopenia of SARS. BMJ **327:** 620–626
40 Nicholls J. M., Poon L. L., Lee K. C., Ng W. F., Lai S. T., Leung C. Y. at al. (2003) Lung pathology of fatal severe acute respiratory syndrome. Lancet **361:** 1773–1778
41 Maaser C., Eckmann L., Paesold G., Kim H. S. and Kagnoff M. F. (2002) Ubiquitous production of macrophage migration inhibitory factor by human gastric and intestinal epithelium. Gastroenterology **122:** 667–680
42 Beijing Group of National Research Project for SARS (2003) Dynamic changes in blood cytokine levels as clinical indicators in severe acute respiratory syndrome. Chin. Med. J. **116:** 1283–1287
43 Wong C. K., Lam C. W., Wu A. K., Ip W. K., Lee N. L., Chan I. H. et al. (2004) Plasma inflammatory cytokines and chemokines in severe acute respiratory syndrome. Clin. Exp. Immunol. **136:** 95–103